Pharm Res (2014) 31:2054–2064
DOI 10.1007/s11095-014-1307-5

RESEARCH PAPER

# A Complementary Strategy for Enhancement of Nanoparticle Intracellular Uptake

Yingjia Li • Ge Wen • Dongxiao Wang • Xia Zhang • Yaoyong Lu • Jianguo Wang • Lijuan Zhong • Hongbing Cai • Xingmei Zhang • Ying Wang

Received: 4 October 2013 / Accepted: 14 January 2014 / Published online: 21 February 2014


## ABSTRACT

***Purpose*** The complementary strategy by combining targeting ligand-mediated selectivity and CPP-mediated transmembrane function could be exploit synergies for enhancing cellular uptake of nanoparticles with negative charge. A heparin-based nanoparticles with negative charge was fabricated by complementary strategy, which was expected to attain efficient uptake and simultaneously exert great anticancer activity.

***Methods*** We synthesized heparin-based nanoparticles with targeting ligand folate and CPP ligand Tat to deliver paclitaxel (H-F-Tat-P NPs). The NPs were characterized by $^{1}$H NMR, DLS and TEM, respectively. The effect of dual ligands on system behavior in aqueous solution was investigated. Moreover, its cellular internalization and anticancer activity were detected by flow cytometry, confocal microscopy and MTT.

***Results*** Folate played a key role in the formation of heparin-based NPs dependent on the balance of amphiphilic Tat and hydrophobic folate. Although H-F-Tat-P NPs primarily entered FR specific and non-specific cells by similar routes, there were no comparability due to cell-type specific variation. Unlike non-specific cells, the complementary ligands could help negative-charged NPs to enhance cellular uptake facilitating its endosome escape in specific cells thereby exhibiting great anticancer activity.

***Conclusions*** The complementary strategy for negative-charged NPs was presented a promising delivery system for diverse anticancer agents enable simultaneously targeting and drug delivery.

**KEY WORDS** complementary ligands · intracellular uptake · nanoparticles · negative charge

## ABBREVIATIONS

| | |
|---|---|
| H-F-Tat-P NPs | Heparin-Folate-Tat-Paclitaxel Nanoparticles |
| FR | Folate Receptor |
| Tat | Transactivating transcriptional activator peptide |
| CPP | Cell-penetrating peptide |
| MBCD | Methyl-β-cyclodextrin |
| CPZ | Chlorpromazine |
| DLS | Dynamic light scattering |
| TEM | Transmission electron microscope |

## INTRODUCTION

Polymeric nanoparticles have received much attention in drug delivery systems due to their diverse surface chemistry, appropriate size scale and unique pharmcokinetics, which make them combine and deliver several functionalities simultaneously and specifically to tumor site (1,2). Heparin is a natural polysaccharide with biocompatibility, biodegradability, and water-solubility. Beside its well-known anticoagulant property, heparin has numerous important biological activites interacting with proteins in application of heparin-containing systems (3,4). It can exert antitumor activities in the tumor

Y. Li • Y. Lu • J. Wang • L. Zhong • Y. Wang (✉)
Cancer Research Institute, School of Basic Medical Sciences
Southern Medical University, Guangzhou 510515, China
e-mail: ningmengquan@gmail.com

Y. Li • D. Wang • X. Zhang
Department of Ultrasonography, Nanfang Hospital
Southern Medical University, Guangzhou 510515, China

G. Wen
Imaging Center, Nanfang Hospital
Southern Medical University, Guangzhou 510515, China

H. Cai
School of Traditional Chinese Medicine
Southern Medical University, Guangzhou 510515, China

X. Zhang
Department of Neurobiology, School of Basic Medical Sciences
Southern Medical University, Guangzhou 510515, China

progression and metastasis (5–7). Therefore, the development of heparin-based nanoparticles has significant implications for cancer therapy. Although several recent attempts to explore heparin-based nanoparticles involve combining targeting moieties and therapeutic agents, the strategies mainly present single specific ligand (for example folate) to decorate heparin backbone for drug delivery systems (8–11). A more effective targeting system has been damanded to enhance drug intracellular uptake and further improve therapeutic effect. Potentially, cellular uptake and selectivity of nanoparticles can be improved by the introduction of functional ligands promoting cell binding and internalization. Therefore, it will be desirable to fabricate multifunctional heparin-based nanoparticles thereby enhancing its internalization ability by surface functionalization.

Many functionalized nanoparticulate strategies have employed various of ligands with complementary function to present great cellular internalization, for example targeting ligands (to induce cell surface adhere and receptor-mediated endocytosis) and endosomal escape ligands (to imporve delivery to cytosol and escape endolysosomal degradation) (12). Among them, folate can selectively bind to folate receptor (FR) of cell-surface significantly upregulated in malignant tumors and has been served as a targeting moiety to differentially deliver anticancer drugs (13–17). Transactivating transcriptional activator peptide (Tat) is a well-studied cell-penetrating peptide (CPP), another commonly utilized class of ligands capable of facilitating the efficient uptake of cargos ranging from small peptide sequences to large biomolecules (18–21). However, a significant hindrance for its potential applications *in vivo* is lack of targeting selectivity in cell entry. Hence, the combination of FR-mediated selectivity and CPP-mediated transmembrane ability may be a complementary strategy for production of new drug delivery system for further application. Many research groups have reported nanoparticles with folate and Tat dual-ligand (12,22,23) displayed positive or neutral charge based on the successful transduction coming from direct contact between the positive charge of Tat and the negative charge in cell surface (20,24). But the application of positive-charged NPs can easily cause significant toxic effect (25,26). In addition, although the majority of NPs are accumulated in the organs of reticuloendothelial system (RES) after intravenous injection (i.v.), it has reported that slightly negative-charged NPs can reduce nonspecific uptake in liver and spleen to some extent attributed to the electrostatic repulsion between negative-charged NPs and cellular surface of RES organs (27,28). Therefore, the development of negative-charged NPs with good internalization ability is highly desirable. Although the negative-charged NPs is unfavorable CPPs' exertion of transmembrane function, the complementary strategy by combining the targeting ligand-mediated selectivity and CPP-mediated transmembrane function may facilitate negative-charged NPs to efficiently deliver therapeutic agents thereby enhancing their cellular internalization.

We have previously reported the fabrication of folate-targeted heparin-based nanoparticles to deliver paclitaxel (29). Using incorporation of folate at the distal end of PEG, the nanoparticles can be differentially delivered to FR specific cells. However, due to the structure of PEG, the introduced amount of folate in PEG may be too low to exhibit a greater intracellular uptake. In this study, we have fabricated dual-functionalized NPs composed of heparin-based polymer conjugated with folate and Tat peptide to differentially deliver paclitaxel (H-F-Tat-P NPs) (Fig. 1). Paclitaxel delivery by such construction can be attractive to improve its uptake, as it would take profit of complementary function from targeting ligand-mediated selectivity and CPP-mediated internalization ability. To the best of our knowledge, no one has thus far, utilized folate and Tat dual functionalities to decorate negative-charged heparin resulting in the enhancement of intracellular uptake thereby exhibiting significant anticancer activity. In addition, studies reported in the literatures folate conjugation to the polysaccharide promoted the formation of self-assembly nanoparticles (30,31); however, it is unknown the influence of folate combining with amphiphilic peptide on system self-assembly behavior. Herein, we have investigated the effect of dual functionalities on system behavior in aqueous solution; moreover, we have aimed to explore its intracellular trafficking of dual-functionalized NPs. Particularly, it is necessary to test the cellular uptake pathway of negative-charged NPs with complementary ligand as well as the colocalization of NPs with endocytosis marker in cells. The work may provide useful information about construction of selected intracellular compartments.

## MATERIALS AND METHODS

### Materials

Heparin sodium salt (Mn=1.25 kDa, 189 U/mg) was purchased from Sinopharm Chemical Reagent Co. (Shanghai, China). Oregon green488 cadaverine was obtained from Invitrogen Co. 4-dimethylaminopyridine (DMAP), N-hydroxysuccinimide (NHS) and 1-ethyl-3,3-dimethylaminopropylcarbodiimide hydrochloride (EDC), and were purchased from Medpep Co. (Shanghai, China). Seven hundred thirty-two cation-exchange resins were purchased from Shanpu Co., Ltd. (Shanghai, China). Paclitaxel was obtained from Tianfeng Co. (Shenyang, China). TAT peptide (Tyr-Gly-Arg-Lys-Lys-Arg-Arg-Gln-Arg-Arg-Arg, Mw 1,560 Da) was synthesized by ChinaPeptides Co. Ltd. (Shanghai, China). All other chemicals and reagents were from Sigma Co. Folate-$NH_2$ was prepared in our lab. Spectra/Por 3 Dialysis Membrane (MWCO 3,500) was from Pharmacia (Piscataway, NJ). Ultrapure water (Mili-Q, 18 M • Ω ) was used in the experiment.

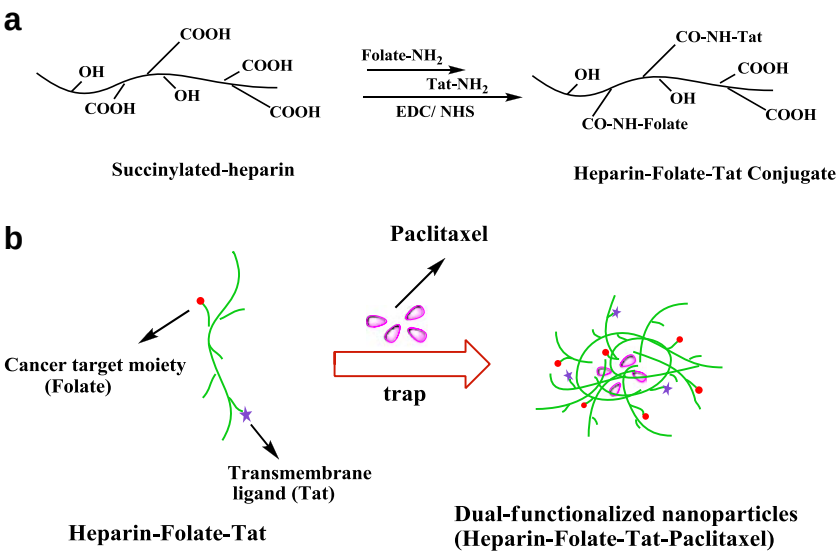


**Fig. 1** Designed strategy of dual-functionalized nanoparticles, (**a**) Preparation of Heparin-Folate-Tat conjugate (H-F-Tat), (**b**) Preparation of Heparin-Folate-Tat-Paclitaxel nanoparticles (H-F-Tat-P NPs).

## Synthesis of Succinylated-heparin

Succinylated-heparin was synthesized by previous method (29). Briefly, 0.25 g of heparin in water was passed through a $H^+$ 732 column at low temperature. Its pH was adjusted to 6.0 by addition of tributylamine and excess tributylamine was evaporated. The concentrate was dissolved in water and lyophilized to produce 0.5 g of heparin tributylammonium salt. The 0.5 g of tributylammonium salt in dry DMF was cooled down to 0°C. Succinic anhydride (1.3 g, 13 mmol), DMAP (0.036 g, 0.3 mmol) and triethylamine (1.31 g, 13 mmol) were added and reacted at room temperature for 24 h. The solvent was evaporated and the concentrate dissolved in a little water followed by passing through a $H^+$ 732 column. The collected solution was dialyzed by a membrane (MWCO 3,500). Then solution was neutralized and lyophilized as a white powder (0.20 g). $^1$H NMR ($D_2O$): $\delta$ = 2.5 ppm ($-CH_2CH_2COOH$, succinylated group).

## Synthesis of Heparin-Folate-Tat (H-F-Tat)

Succinylated-heparin in dry DMSO was stirring by gentle heating. Some amount of Folate-$NH_2$, Tat peptide, EDC and NHS were mixed and reacted at room temperature for 24 h. The deionized water was then added and dialyzed in a dialysis membrane. The solution was then lyophilized and obtained a yellow powder. Oregon green488-labled H-F-Tat was synthesized by a similar procedure as that of H-F-Tat. $^1$H NMR ($D_2O$): δ 2.8 ppm ($-CH_2CH_2COOH$, succinylated-heparin), 6.8 and 7.6 ppm (folate).

## Preparation of Heparin-Folate-Tat-Paclitaxel NPs (H-F-Tat-P NPs)

NPs were prepared by a nano-precipitation method with minor modifications (32). H-F-Tat and paclitaxel was mixed in dry DMSO at 35°C for 6 h. The mixture was dialyzed by a dialysis memberane (MWCO 3,500) for 48 h. The excess water was concentrated followed by filtering through a 450 nm membrane. The H-F-Tat-P NPs was lyophilized and obtained a light yellow powder. $^1$H NMR ($D_2O$): δ 2.8 ppm ($-CH_2CH_2COOH$, succinylated-heparin), 6.8 ppm, 7.6 ppm (folate). (DMSO-$d_6$): δ 1.02 ppm (17,16-$CH_3$, taxol), 1.51 ppm (19-$CH_3$, taxol), 1.78 ppm (18-$CH_3$, paclitaxel), 2.09 ppm (C4-OAc, paclitaxel), 2.21 ppm (C10-OAc, paclitaxel), 7.2 ~ 8.0 ppm (benzene ring, paclitaxel).

## Characterization

The $^1$H NMR spectra of the product were determined by a Bruker-400 MHz NMR in DMSO-$d_6$ and $D_2O$. The weight of the succinlyated group was quantitatively analyzed by $^1$H NMR using pyridine as an internal standard, whose pyridine signals are δ 7.4, 7.9 and 8.4 ppm. The weight of folate on H-F-Tat was caculated by UV spectrometer (UV-2,401, Shimadzu) based on a folate standard curve of concentration-absorption at 366 nm. The amount of Tat was determined using UV method by quantifying the FITC-labeled Tat based on a FITC-labeled Tat standard curve of concentration-absorption at 488 nm. The content of paclitaxel was determined by HPLC based on paclitaxel standard curve. H-F-Tat-P were dissolved in water and stirred gently. The aliquots were extracted by chloroform three times and then the organic fraction was concentrated. The residue was mixed with 1 mL of methanol analyzed by HPLC (Waters 2,487 series) using a C18 silica column (4.6× 250 mm, 5 μm, Kromasil), a mobile phase of acetonitrile : 0.2% phosphoric acid in water (76: 24) pumped at a flow rate of 1.0 mL/ min. A 30 μL sample was injected, and the effluent was detected at 227 nm by a UV detector. The encapsulation efficiency (E.E.%) were calculated by equation: amount

of paclitaxel in nanoparticles / initial amount of paciltaxel×100%.

Zeta potentials and size distributions of NPs were detected at 25°C by dynamic lighting scattering (DLS) using a Zetasizer Nano-Zs (Malvern Instruments, UK). The concentration of samples in different condition was constant at 0.3 mg/mL. The morphology of NPs was detected by Transmission electron microscope (TEM, Hitachi HC-1, 80 KV) following negative staining with phosphotungstic acid.

The *in vitro* release of NPs was measured in PBS (pH=7.0) containing 0.1% Tween-80 using the dialysis method. Briefly, 2 mL of NPs solution was suspended in a dialysis bag (MWCO 3,500), and the bag was then immersed in PBS (48 mL) and shaken horizontally (100 rpm) at 37°C. At predetermined intervals, 1 mL aliquots were withdrawn and replaced with an equal volume of fresh PBS. The concentration of paclitaxel in the collected samples was analyzed using HPLC according to the above chromatographic conditions.

## Cell Culture

A human breast carcinoma cell lines, MDA-MB231 cells (FR specific cell lines), and a human lung epithelial carcinoma cell lines, A549 cells (FR non-specific cell lines) were come from ATCC. MDA-MB231 cells and A549 cells were cultured L-15 and RPMI 1,640 in 5% $CO_2$ at 37°C, respectively. The culture media were supplemented with 10% fetal bovine serum, 100 units/mL penicillin/streptomycin and 2 mmol/L glutamine.

## Cellular Uptake Studies of NPs

Oregon green488 labeled H-F-P NPs and H-F-Tat-P NPs were synthesized by the similar procedure as above described. The weight percentage of folate and paclitaxel was about 15.45% and 12.1% in Oregon green488 dye-labeled H-F-P NPs. MD-MBA-231 cells were plated in 6-well plates at a density of $2.5\times10^5$ cell per well in medium and incubated for 24 h. All uptake experiments were in serum free medium. The temperature blocking experiment was pre-incubated MD-MBA-231 cells at 4°C for 1 h and treated with Oregon green488 labeled H-F-P NPs and H-F-Tat-P NPs for 1 h at 4°C. To test the effects of endocytosis inhibitors on the cellular uptake of NPs, MD-MBA-231 cells were pre-incubated for 1 h at 37°C with 50 μM of amiloride to inhibit macropinocytosis, 200 μM of genistein to inhibit lipid-raft mediated caveolae, 10 mM of methyl-β-cyclodextrin (MBCD) to inhibit caveolae, and 10 μg/mL of chlorpromazine (CPZ) to inhibit the formation of clathrin vesicles, and then treating the cells with Oregon green-488 labeled H-F-P NPs and H-F-Tat-P NPs for an additional 1 h. Next, to eliminate trace product the incubated cells were washed three times by cold PBS, and detached with EDTA-PBS and then suspended in PBS (0.1% BSA). The suspended cells were directly detected a FACSort flow cytometer (Becton Dickinson, USA) equipped with a 488 nm argon ion laser. Data for 10,000 fluorescent events were obtained by recording forward scatter and side scatter with 530/15 nm fluorescence. The autofluorescence of cells was taken as a control.

In order to visualize nanoparticles colocalization with lysosomes, MDA-MB231 cell lines and A549 cell lines were incubated in the chambered slide. Cells were washed with PBS after treatment of Oregon green488 labeled NPs for 4 h and then incubated with Lysotracker-Red for an additional 30 min. The cells were fixed using 4% (w/v) *para*-formaldehyde solution followed by Hochest33342 staining. The fluorescence images were observed by confocal microscope (Olympus FV1000, Japan).

To investigate the cellular uptake of carrier with single targeted ligand and dual ligands, DiI as model drug was entrapped into H-F and H-F-Tat to detect drug release into MDA-MB-231 cells. MDA-MB-231 cells were incubated with H-F-DiI NPs and H-F-Tat-DiI NPs for 4 h. The treatment method was the same as the previous colocalization study.

## MTT Assay for Cell Viability

MDA-MB-231 were reseeded in 96-well plate at an initial density of $4\times10^3$ cells/well in 200 μL RPMI1640 containing 10% FBS at 37°C in humidified 5% $CO_2$. After incubated with 24 h, the culture medium/ per well was replaced with 200 μL fresh medium containing different concentrations of free paclitaxel and H-F-Tat-T NPs. 24 h later, the media were detached and replaced with 25 μL of MTT solution (1 mg/mL) followed by incubation for 4 h. Then, the solution was replaced with DMSO and the plates were slightly shaken. The plate was detected at 570 nm using a microplate reader (Biotek, USA). Cells without samples were taken as the control.

## Flow Cytometric Detection of Cell Cycle

MDA-MB-231 cells were seeded on a 6-well plate and incubated for 24 h. And then cells were coincubated with paclitaxel and H-F-Tat-P NPs (an equivalent drug concentration of 30 μg/mL) for 6 h. The cells were washed and detached by trypsinization followed by spining down by centrifugation and dispersing in PBS. The cells were fixed in 70% ethanol /PBS (10:1) for 1 h and washed with PBS, and then stained by PI and RNase. The cell cycle of suspended cells was analyzed by a flow cytometer.

## Statistical Analysis

Statistical analysis was made to determine differences between the measured properties in each group. One-way analysis of

variance was analyzed by a statistical program (SPSS, 10.0 V, SPSS Inc., USA). All of data were processed in triplicate or sextuplicate and showed a mean value with standard deviation (mean±SD.)

## RESULTS

### Preparation and Characterization of H-F-Tat-P NPs

The H-F-Tat conjugate was initially synthesized by a coupling reaction between the amine groups of aminated folate and Tat and the carboxyl groups of succinlyated-heparin obtained from O-acylation. Next H-F-Tat conjugate displayed an amphiphilic property capable of physically entrapping with hydrophobic anticancer drug paclitaxel by necessary chemical modification of heparin (Fig. 1). Nanoparticles were prepared using a nano-precipitation method (32).

The typical $^1$H NMR spectra of H-F-Tat in DMSO-$d_6$ and $D_2O$ are presented in Fig. 2a and b. It showed peak signal at 2.7 ppm and weak signals at 6.8 ppm and 7.6 ppm attributed to the succinylated group in heparin and the fraction of folate, respectively. Although the partial structure of Tat could be observed in both solvents, it was hard to clearly attribute due to its complex structure thereby requiring other characterized method.

Direct proofs confirming drug entrapped into H-F-Tat come from Fig. 2c and d. Part of paclitaxel structure could be detected at peaks from 5 to 9 ppm in DMSO-$d_6$. Interestedly, paclitaxel peaks disappeared while the proton peaks at 6.8 and 7.6 ppm corresponded to folate in $D_2O$. The weight percentage of succinylate groups was about 15% in heparin by $^1$H NMR analysis, indicating that sufficient carboxyl groups could raise reaction activity. Figure 2e presents UV spectrum of H-F-Tat conjugate. Clearly, the characterized absorption peak of folate appeared at 276 nm and 366 nm in H-F-Tat conjugate. To quantitatively analysis Tat, we selected Tat labeled with FITC as materials and the UV spectrum of H-F-FITC/Tat conjugate were measured, wherein the absorption peaks of folate were sheltered by FITC signal appearing around 500 nm in Fig. 2f.

To investigate the effect of dual-functionalities on system self-assembly behavior, we prepared H-F-Tat1 and H-F-Tat2 with different folate and Tat ratio to entrap paclitaxel (H-F-Tat-P1 NPs and H-F-Tat-P2 NPs) and their characterization was shown in Table I. It was found when the content of folate and Tat was about 8.4% and 5.5%, H-F-Tat-P1 NPs contained about 8.3% paclitaxel and the encapsulation efficiency was about 95%; however H-F-Tat2 didn't display encapsulation ability as good as H-F-Tat1. We also test the stability of two NPs in different condition by DLS. It was shown in water the size of H-F-Tat-P1 NPs and H-F-Tat-P2 NPs was around 78 nm and 101 nm respectively, but both of them displayed increased trend in different PBS solution; especially, their zeta potential changed from around −32 mV in water to −17 mV in PBS, indicating the polymer charge involved in self-assemble process of NPs formation and the addition of ionic could as well affect it. To further observe the morphology of two NPs, TEM images of H-F-Tat-P1 NPs and H-F-Tat-P2 NPs were taken (Fig. 3a and b). H-F-Tat-P1 NPs clearly displayed an approximately spherical shape, while only a small part of H-F-Tat-P2 NPs were observed and most of them displayed compromised morphology difficult to identify particle shape. The controlled release kinetics of paclitaxel from H-F-Tat-P1 NPs and H-F-Tat-P2 NPs is shown in Fig. 3c. H-F-Tat-P2 NPs displayed a slightly faster release rate than H-F-Tat-P1 NPs. Approximately 30% of paclitaxel from NPs was released at the initial 18 h of dialysis. After 72 h, both of them had released about 60% of paclitaxel into PBS, indicating a slow release of H-F-Tat-P NPs.

### Cellular Uptake Mechanism of NPs

Based on the complexity of H-F-Tat-P NPs, it was necessary to precisely delineate the role of individual factor on cellular uptake. We first synthesized Oregon green488 labeled H-F-P NPs and H-F-Tat-P NPs and tested the cellular uptake of these NPs in presence of specific inhibitors (Fig. 4). We could not conduct the intracellular uptake experiments of H-Tat-P NPs due to lack of its optimal formulation. A549 cells and MDA-MB-231 cells were employed as FR overexpressing and deficiency cancer cells treated with Oregon green488 labeled NPs and evaluated the effect of individual ligand, dual ligands and negative-charged NPs.

Regard to A549 cells, the internalization of H-F-P NPs was decreased in presence of MBCD and genistein, the inhibitors of caveloae. Along with the introduction of Tat, we found the internalization of H-F-Tat-P NPs was blocked by multiple inhibitors (MBCD, genistein and CPZ); furthermore the MBCD inhibition was enhanced compared with that of H-F-P NPs (Fig. 4a). In view of FR overexpressing MDA-MB-231 cells, the uptake of H-F-P NPs was restricted by multiple inhibitors and the order of inhibition was MBCD>CPZ>genistein. Interestedly, despite of the addition of Tat, internalization of H-F-Tat-P NPs was suppressed by the same inhibitors as that of H-F-P NPs, wherein the inhibition of MBCD and CPZ was strengthened and the inhibition of genistein (>80%) could be negligible compared with that of H-F-P NPs (Fig. 4b). Additionally, incubation of all NPs at 4°C for 1 h resulted in an inhibition of endocytosis, and the cellular uptake of H-F-Tat-P NPs was affected more but still significantly compared with that of H-F-P NPs against both cells. Note that amiloride , the inhibitor of macropinocytosis, had no significant effect in case of H-F-Tat-P NPs and H-F-P NPs.

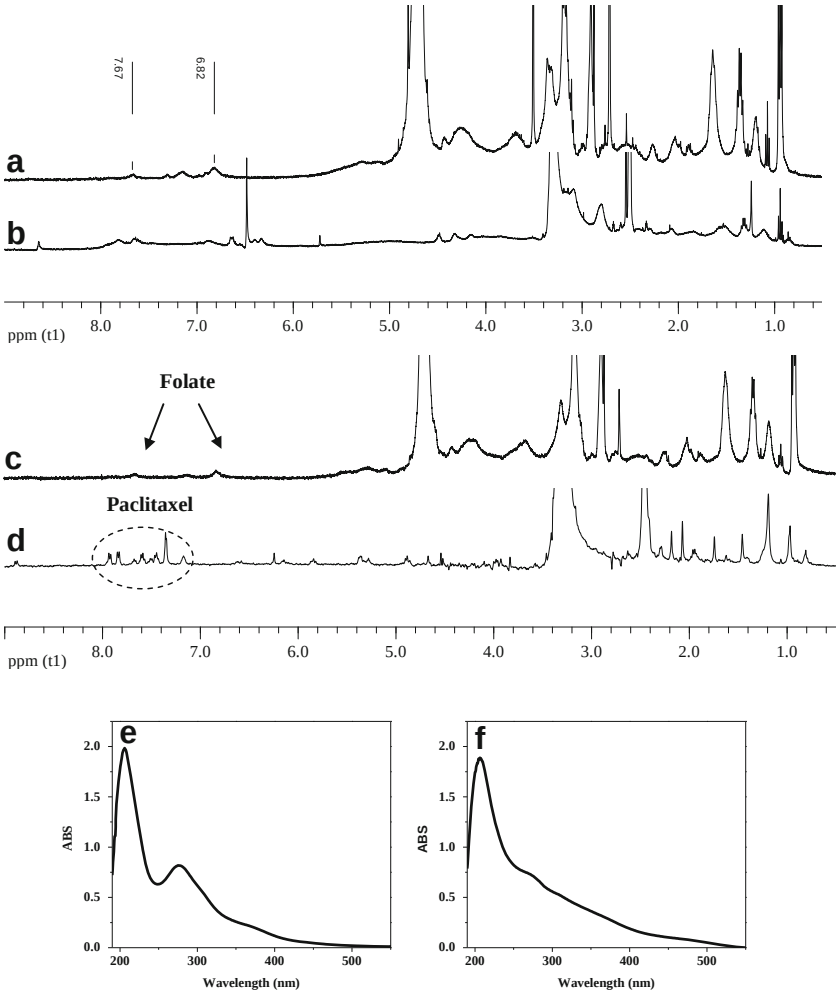


**Fig. 2** $^1$H NMR spectra of H-F-Tat conjugate in (**a**) DMSO-$d_6$ and (**b**) $D_2O$; H-F-Tat-P NPs in (**c**) $D_2O$ and (**d**) DMSO-$d_6$; UV spectra of (**e**) H-F-Tat conjugate and (**f**) H-F-FITC/Tat conjugate.

**Table I** Characterization of H-F-Tat-P NPs

| NPs | H-F-Tat-P1 NPs | H-F-Tat-P2 NPs |
|---|---|---|
| Folate loading weight (w/w %) | 8.4 ± 1.5 | 13.45 ± 2.4 |
| Tat loading weight (w/w %) | 5.5 ± 0.7 | 3.1 ± 0.4 |
| Paclitaxel loading weight (w/w %) | 8.3 ± 0.6 | 5.36 ± 1.7 |
| Encapsulation efficiency (w/w %) | 95 ± 1.4 | 68 ± 2.5 |
| Mean diameter (nm) | | |
| Water | 78 ± 7 | 101± 5 |
| PBS (5.8) | 82 ± 4 | 110 ± 7 |
| PBS (7.0) | 84 ± 7 | 114 ± 5 |
| PBS (8.0) | 90 ± 4 | 117 ± 3 |
| Zeta (mV) | | |
| Water | −32 ± 5 | −35 ± 3 |
| PBS (5.8) | −15 ± 2 | −16 ± 2 |
| PBS (7.0) | −16 ± 1 | −15 ± 3 |
| PBS (8.0) | −16 ± 2 | −18 ± 2 |

Data were presented as means±SD, $n=3$

## Colocalization Study

Here, to elucidate the intracellular localization of H-F-Tat-P NPs, MDA-MB-231 cells and A549 cells were treated with Orgeon green488 labeled H-F-Tat-P NPs for 4 h, and then exposure with Lysotracker Red probe for 30 min. The position of nucleus in each cell was labeled with Hochest33342 staining (blue). The confocal laser scanning microscopy images of MDA-MB-231 cells and A549 cells are shown in Fig. 5. It could be observed the colocalization of H-F-Tat-P NPs with lysosome produced a yellow fluorescence in merged images. Regard to MDA-MB-231 cells, some of Oregon green488 labeled NPs adhered to the cytoplasm and lysosome caused yellow fluorescent signal, especially it was clearly observed a part of green nanoparticle spots distributed in nucleus (Fig. 5a). However, most of Oregon green488 labeled H-F-Tat-P NPs was distributed in the cytoplasm and represented yellow fluorescence merged with lysosome in A549 cells (Fig. 5b).

In order to evaluate the ligand effect of NPs on cellular uptake, we designed DiI as model drug entrapped into H-F

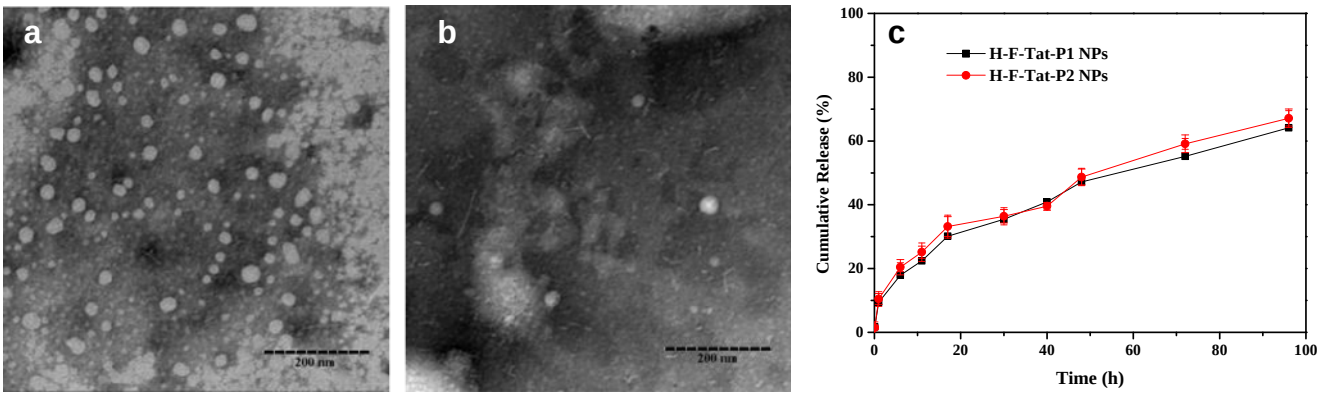


**Fig. 3** Transmission electron microscopy photograph of (**a**) H-F-Tat-P1 NPs and (**b**) H-F-Tat-P2 NPs; (**c**) The controlled-release kinetics of H-F-Tat-P1 NPs and H-F-Tat-P2 NPs in PBS (pH 7.0).

and H-F-Tat conjugate and detected its location in FR specific cells (Fig. 6). It was obviously detected model drug DiI was located in cytoplasm of cells treated with NPs with single targeting ligand, while the red fluorescent signal was observed in not only cytoplasm but also nucleus of cells in exposure with NPs with dual complementary ligands (Fig. 7).

### *In Vitro* Assay

We performed cytotoxicity experiments of free paclitaxel, H-F-P NPs and H-F-Tat-P NPs against MDA-MB-231 cells. In comparison with that of paclitaxel and H-F-P NPs, H-F-Tat-P NPs exhibited greater cytotoxicity ($IC_{50}$ 45.8 μg/mL). Also, in absence of Tat transmembrane function H-F-P NPs was not complete but effective to kill the specific cells. To examine dual-functionalized NPs effect on cell cycle, MDA-MB-231 cells were treated with NPs and positive control free paclitaxel for 6 h. The control cell cycle distribution displayed 18.65% of the cells were in the G2/M phase, while it was increased to 36.93 and 32.83% for paclitaxel and H-F-Tat-P NPs treated MDA-MB-231, respectively.

## DISCUSSION

Accumulating documents showed that NPs with positive charge could easily enter cells due to its electrostatic attraction with the negative-charged plasma of cells, but the positive-charged NPs might cause higher toxic effect compared with the negative-charged (25,26). In particular, it was reported that negative-charged NPs would be advantageous for cancer therapy due to its reduced plasma protein adsorption and low rate of non-specific cellular uptake (28). Therefore, it was expected to fabricate efficient negative-charged NPs enhancing their cellular internalization and simultaneously exerting great anticancer activity. Over the last years, CPPs were widely exploited for the intracellular delivery of different cargoes (18,20,33). The direct electrostatic interaction between the positive charge of Tat and negative charge of cell-surface proteoglycans was a prerequisite for the transduction of Tat (20,24). Accordingly, the conjugation of Tat to negative-charged carrier was not conducive to its cellular uptake. However, complementary strategy by combining targeting ligand-mediated selectivity and CPP-mediated internalization function could be developed synergies for enhancing cellular uptake of negative-charged NPs. Hence, we

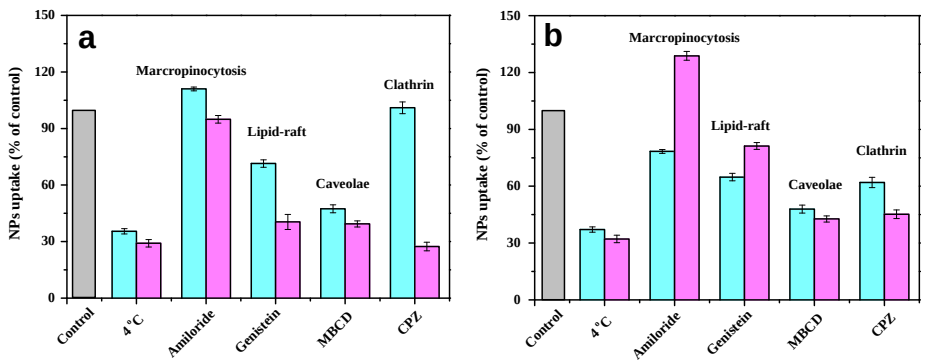


**Fig. 4** Investigation of the mechanisms of cellular internalization by using inhibitors of endocytosis. (**a**) A549 cells and (**b**) MDA-MB-231 cells were incubated with (□) H-F-P NPs and (□) H-F-Tat-P NPs for 1 h. Cells were incubated either at 37°C or 4°C. Prior to the incubation with NPs, cells were pretreated with amiloride, genistein, methyl-β-cyclodextrin (MBCD) or chlorpromazine (CPZ). The internalization ratio was normalized to that of the control (internalization of NPs in the absence of inhibitors).

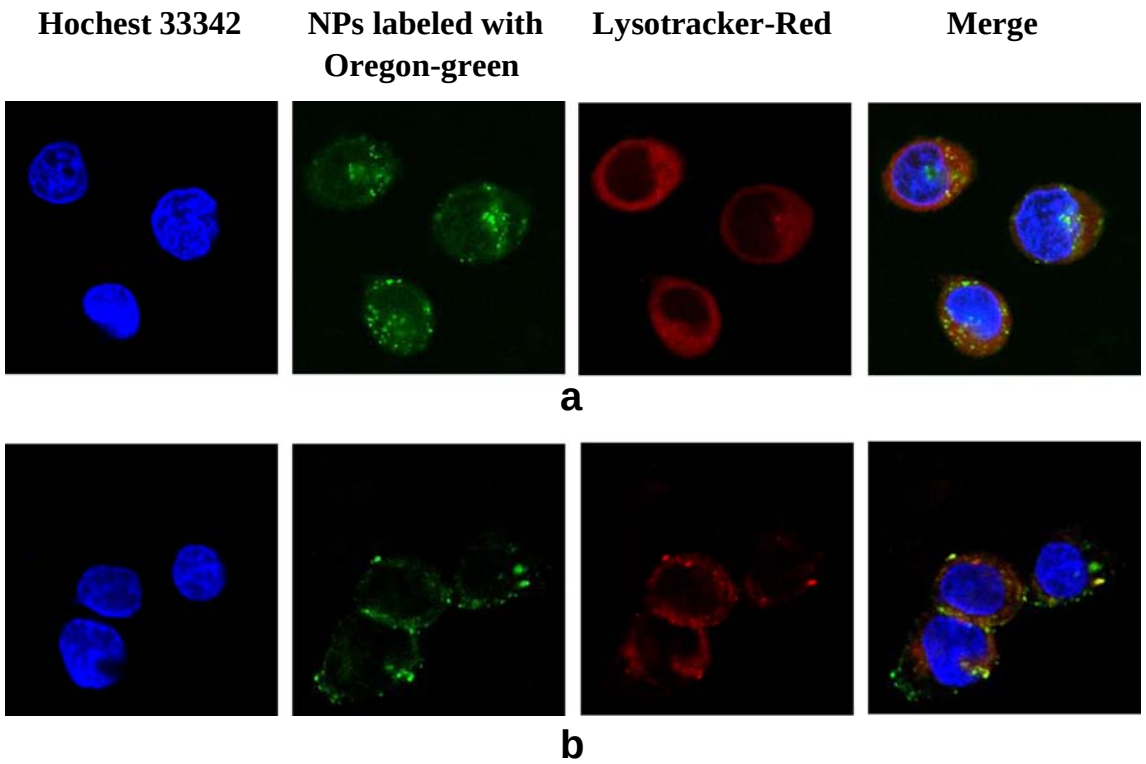


**Fig. 5** Confocal microscopic images of (**a**) MDA-MB-231 cells and (**b**) A549 cells after 4 h incubation with H-F-Tat-P NPs, and then incuabated with Lysotracker-Red. The *left images* were nucleus staining by Hochest33342 (*blue*); the second were cell treated with Oregon green488 labeled NPs (*green*); the third were cell treated with Lysotracker-Red; the *right* were merged pictures from previous three. ×60.

designed heparin-based NPs with dual functionalities to differentially delivery paclitaxel (H-F-Tat-P NPs) and investigated its potential feasibility for tumor-targeted drug delivery. Negative-charged NPs was expected to attain

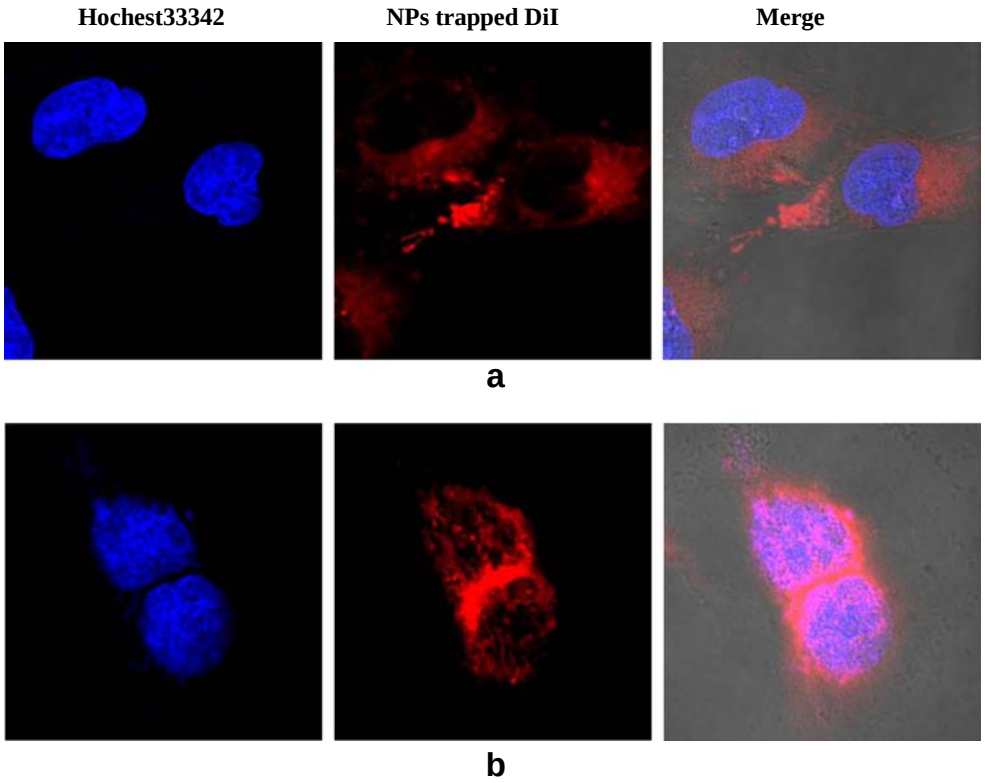


**Fig. 6** Confocal microscopic images of MDA-MB-231 cells after 4 h incubation with (**a**) H-F-DiI NPs and (**b**) H-F-Tat-DiI NPs. The *left* images were nucleus staining by Hochest33342 (*blue*); the second were cell treated with NPs with DiI (*red*); the *right* were merged pictures from previous two and bright field. ×60.

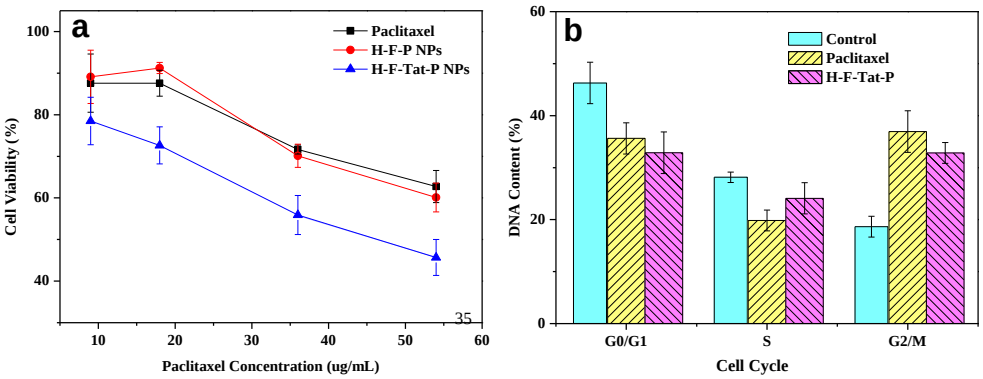


**Fig. 7** (**a**) Cell viability of MDA-MB-231 cells after treatment with free paclitaxel, H-F-P NPs and H-F-Tat-P NPs for 24 h. (**b**) Cell cycle was determined by flow cytometric detection of MDA-MB-231 cells treated with free paclitaxel and H-F-Tat-P NPs for 6 h. The results represent the mean±SD, $n=6$.

efficient uptake with aid of targeting ligand, transmembrane peptide and nanoparticles size effect.

It was shown that the introduction of amphiphilic molecules to heparin could benefit to its lipophilic property improvement (29). As depicted in Fig. 2, H-F-Tat structure could be identified in DMSO-$d_6$ and $D_2O$, suggesting H-F-Tat displayed amphiphilic property. In addition, partial structure of folate and paclitaxel was appeared in both solvents, suggesting the carrier was oriented outside with exposing folate and Tat capable of entrapment of paclitaxel in aqueous solution. As such, H-F-Tat-P could self-organize into core/shell type nanoparticle.

Park K et al reported folate conjugation to the heparin backbone promoted the formation of self-assembled nanoparticles (11). Meanwhile, we found the self-assembled behavior of heparin-folate conjugate occured using a sufficient amount of folate in accordance with Nie's report (34). Hence, we synthesized H-F-Tat1 and H-F-Tat2 conjugates with different folate and Tat ratio and examined their encapsulation ability. In addition, in view of the selectivity of NPs, we couldn't discuss H-F-Tat conjugate with lower folate content. Although it was found that both of them had self-assembled behavior in aqueous solution by DLS, the encapsulation ability of H-F-Tat2 wasn't as good as H-F-Tat1; in addition, H-F-Tat-P1 NPs and H-F-Tat-P2 NPs appeared obviously different morphology in TEM. Tran et al reported the presence of folate favored the encapsulation of hydrophobic molecule into heparin-based conjugate (30). The peptides generally displayed amphiphilic property, but Tat peptide contained more hydrophilic amino acid sequences resulting in unfavorable entrapment of hydrophobic molecules into heparin. Therefore, in comparison with the physicochemical property of folate and Tat, the introduction of folate played a major role in the formation of heparin-based NPs. It was also confirmed by our experiment that H-Tat conjugate displayed bad encapsulation capacity and formed the larger size particles (300~600 nm) (data not shown). Interestedly, H-F-Tat-P2 NPs could not self-organize optimal nanoparticles, demonstrating the blind increase of folate content might cause self-assemble behavior restriction. As such, the formation of heparin-based NPs was dependent on the balance of amphiphilic Tat peptide and hydrophobic folate. It was worth noting that size of both NPs changed a little bit large and their zeta potential inclined toward positive in PBS compared with those in water, suggesting negative charge of heparin involved in nanoparticles formation resulting in NPs' loosened trend after the replacement of PBS. Accordingly, compared with construction of H-F-Tat-P2 NPs, H-F-Tat-P1 NPs presented compact state thereby producing slightly slower liberated rate in PBS.

Many research groups have reported more than one mechanism works for CPP-mediated intracellular delivery of small and large molecules, including the clathrin-mediated endocytosis, caveoloae-mediated clathrin-independent endocytosis, the lipid-raft-mediated caveoloae endocytosis and macropinocytosis, etc (20). A widely held view was FR-mediated intracellular pathway primarily involved clathrin-mediated endocytosis in specific cells (35). Considering complementary effect of dual ligands, it was necessary to gain insight into its cellular uptake pathway. Herein, we tested the cellular uptake of H-F-P NPs (Zeta−35 ± 3 mV) and H-F-Tat-P NPs in presence of endocytic inhibitors against FR specific and non-specific cells.

We found cellular uptake of H-F-P NPs was inhibited by MBCD and genistein (caveolae inhibitors) against FR non-specific cells, demonstrating the negative-charged heparin-based NPs was endocytosed *via* a caveolae-pitted mechanism. It was agreed with Zhang's report the negative-charged nanoparticles entered into cells primarily through caveolae-mediated endocytosis (36). Along with the introduction of Tat, H-F-Tat-P NPs was inhibited by not only MBCD and genistein but also CPZ (clathrin inhibitor), indicating the its inhibition pathways were increased (caveolae and clathrin-mediated endocytosis); furthermore the caveolae effect was enhanced compared with that of H-F-P NPs, implying the addition of Tat brought out clathrin and caveolae endocytic pathways. It was suggested that the mechanism of endocytosis for H-F-Tat-P NPs was mediated by caveolae and clathrin corresponding to the effect of Tat and negative-charged nanoparticles.

In contrast, multiple inhibitors (MBCD, CPZ and genistein) affected the uptake of H-F-P NPs treated with FR specific cells, indicating the caveolae and clathrin-mediated endocytosis was attributed to effect of targeting ligand and negative-charged nanoparticles. Irrespective of the effect of Tat, the same inhibitors as that of H-F-P NPs took effect on the internalization of H-F-Tat-P NPs, while note that MBCD and CPZ had enhanced effect on NPs' uptake in accordance with the phenomena of A549 cells. In case of FR specific cells, the internalization pathway of H-F-Tat-P NPs was mediated by caveolae and clathrin endocytosis from a synergistic effect (targeted ligand, tansmenbrane ligand and nanoparticles).

Also, the cellular uptake of all NPs was blocked under 4°C. The low temperature experiments suggested that the prepared NPs entered cells *via* energy-dependent endocytosis. Interestedly, the cellular uptake of H-F-P NPs and H-F-Tat-P NPs was no obvious change in presence of amiloride, indicating the internalization of prepared NPs could not be mediated by macropinocytosis. It might be macropinocytosis occurred CPP-conjugated to large cargoes (MW>30,000 Da) or larger size particles (20). Due to FR effect, internalization of H-F-Tat-P NPs into specific cells was more complex than that of non-specific cells, thus the uptake mechanism of H-F-Tat-P NPs remained unclear in MDA-MB-231 cells. Although these data implied that H-F-Tat-P NPs primarily entered (MDA-MB-231 and A549) cells by similar routes including caveolae-mediated endocytosis and clathrin-mediated endocytosis, there was no comparability due to cell-type specific variation.

Another method to investigate intracellular trafficking of nanoparticles was colocalization study with specific endocytosis markers. Generally, the cellular uptake of NPs was completed by enclosing them into endosomes (37). It was documented that clathrin-mediation could cause the primary endosomes formation consequently forming late endosomes and lysosomes, acidic organelles with low pH values (38). In this experiment, we utilized lysotracker exposure with cells after H-F-Tat-P NPs uptake. As shown in Fig. 5, parts of H-F-Tat-P NPs was detected in nucleus indicating the dual complementary functionalities could help internalization of NPs thereby facilitating its endosomes escape against specific cells. The behavior could be attributed to the folate targeting effect, Tat transmembrane function and nanoparticle effect. The fluorescence microscopic experiments demonstrated the nanoparticles with single folate ligand could not be observed in non-specific cells (31). As for FR non-specific cells, the observation of H-F-Tat-P NPs in cytoplasm resulted in the transmembrane function of TAT peptide. Although the uptake pathway of H-F-Tat-P NPs in MDA-MB-231 cells was similar as that of in A549 cells, the different microscopic observation could be due to the effect of targeting ligand. In addition, we selected DiI in place of paclitaxel entrapped into H-F and H-F-Tat, followed by confocal observation to compare the effect of single targeting ligand and dual complementary ligands. In Fig. 6, there was obvious difference between NPs with single targeting ligand and dual ligands; namely, dual functionalities could promote drug uptake into nucleus facilitating NPs endosome escape compared with effect of single targeting ligand. Taken together, with aid of dual functionalities the cellular uptake was strengthened facilitating the enhancement of drug uptake in cells. More importantly, heparin-based NPs with complementary ligand preferred to the specific cells, in which dual ligand function in parallel to enhance cell binding and uptake.

Several reports were proposed to explain the synergistic effect of targeting ligand and CPP ligand on the biological activity of anticancer drugs (12,22,23). To further verify our hypothesis about uptake enhancement of H-F-Tat-P NPs triggered by not only targeting ligand but also transmembrane ligand, we performed cytotoxicity experiments of free paclitaxel, H-F-P NPs and H-F-Tat-P NPs against to FR specific cells. The MTT assay demonstrated higher cytotoxicity of H-F-Tat-P NPs was achieved by enhancement of drug uptake induced by the effect of complementary functionalities. The cytotoxicity of H-F-Tat-P NPs were consistent with the results of intracellular trafficking of H-F-Tat-P NPs by flow cytometry and microscopy, suggesting the targeting nanoparticles with transmembrane function was potentially suitable for specific cancer cell therapy. Paclitaxel was an antimicrotubule agent which could promote the microtubule assembly from tubulin dimers and stabiliz microtubules by preventing depolymerization during the G2 mitotic phase of cell cycle. It was shown that H-F-Tat-P NPs block the cell cycle in G2/M. It was in accordance with Schiff et al. reports indicating paclitaxel in NPs induced the same function as free drug to cause cell cycle arrest in the G2/M and, ultimately, cell death by apoptotic mechanisms (39). The complementary strategy for negative-charged NPs could accelerate internalization of negative-charged NPs thereby enhancing drug concentration in cells and exhibiting significant cytotoxicity. The dual-functionalized NPs represented a promising delivery system for diverse anticancer agents enable simultaneously targeting and drug delivery.

## CONCLUSION

In summary, our data suggested that the complementary strategy for negative-charged NPs could enhance drug uptake efficiency and exhibited great cytotoxicity induced by targeting ligand and transmembrane ligand and nanoparticle effect. It might provide useful information about construction of selected intracellular compartments.

## ACKNOWLEDGMENTS AND DISCLOSURES

Yingjia Li and Ge Wen have equal contribution in this work and are both equally considered as first author. The authors are grateful for financial support by Natural Science Foundation of China (Grant No. 21204036, 81272509, 81371559); Science and Technology Planning Project of Guangdong Province (Grant No. 2011B010400018).

## REFERENCES

1. De M, Ghosh PS, Rotello VM. Applications of nanoparticles in biology. Adv Mater. 2008;20(22):4225–41.
2. Riehemann K, Schneider SW, Luger TA, Godin B, Ferrari M, Fuchs H. Nanomedicine—challenge and perspectives. Angew Chem Int Ed. 2009;48(5):872–97.
3. Chung Y-I, Tae G, Yuk Hong S. A facile method to prepare heparin-functionalized nanoparticles for controlled release of growth factors. Biomaterials. 2006;27(12):2621–6.
4. Nie T, Akins Jr RE, Kiick KL. Production of heparin-containing hydrogels for modulating cell responses. Acta Biomaterialia. 2009;5(3):865–75.
5. Bae KH, Mok H, Park TG. Synthesis, characterization, and intracellular delivery of reducible heparin nanogels for apoptotic cell death. Biomaterials. 2008;29(23):3376–83.
6. Casu B, Guerrini M, Guglieri S, Naggi A, Perez M, Torri G, *et al.* Undersulfated and glycol-split heparins endowed with antiangiogenic activity. J Med Chem. 2004;47(4):838–48.
7. Linhardt RJ, Claude Hudson S. Award address in carbohydrate chemistry. Heparin: structure and activity. J Med Chem. 2003;46(13):2551–64.
8. Li L, Bae BC, Tran TH, Yoon KH, Na K, Huh KM. Self-quenchable biofunctional nanoparticles of heparin-folate-photosensitizer conjugates for photodynamic therapy. Carbohydr Polymer. 2011;86(2):708–15.
9. Li L, Kim JK, Huh KM, Lee YK, Kim SY. Targeted delivery of paclitaxel using folate-conjugated heparin-poly (β-benzyl-l-aspartate) self-assembled nanoparticles. Carbohydr Polymer. 2012;87:2012–8.
10. Kemp MM, Linhardt RJ. Heparin-based nanoparticles. Wiley Interdiscipl Rev: Nanomedicine Nanobiotechnology. 2009;2(1):77–87.
11. Park I-K, Tran TH, Oh I-H, Kim Y-J, Cho KJ, Huh KM, *et al.* Ternary biomolecular nanoparticles for targeting of cancer cells and anti-angiogenesis. Eur J Pharm Sci. 2010;41(1):148–55.
12. Cheng CJ, Saltzman WM. Enhanced siRNA delivery into cells by exploiting the synergy between targeting ligands and cell-penetrating peptides. Biomaterials. 2011;32:6194–203.
13. Campbell IG, Jones TA, Foulkes WD, Trowsdale J. Folate-binding protein is a marker for ovarian cancer. Cancer Res. 1991;51(19):5329–38.
14. Ross JF, Chaudhuri PK, Ratnam M. Differential regulation of folate receptor isoforms in normal and malignant tissues in vivo and in established cell lines. Physiologic and clinical implications. Cancer. 2006;73(9):2432–43.
15. Weitman SD, Weinberg AG, Coney LR, Zurawski VR, Jennings DS, Kamen BA. Cellular localization of the folate receptor: potential role in drug toxicity and folate homeostasis. Cancer Res. 1992;52(23):6708–11.
16. Ulbrich K, Michaelis M, Rothweiler F, Knobloch T, Sithisarn P, Cinatl J, *et al.* Interaction of folate-conjugated human serum albumin (HSA) nanoparticles with tumour cells. Int J Pharm. 2011;406(1):128–34.
17. Zhang Z, Huey Lee S, Feng S-S. Folate-decorated poly (lactide-co−glycolide)-vitamin E TPGS nanoparticles for targeted drug delivery. Biomaterials. 2007;28(10):1889–99.
18. Olson ES, Jiang T, Aguilera TA, Nguyen QT, Ellies LG, Scadeng M, *et al.* Activatable cell penetrating peptides linked to nanoparticles as dual probes for in vivo fluorescence and MR imaging of proteases. Proc Natl Acad Sci. 2010;107(9):4311–6.
19. Rao KS, Reddy MK, Horning JL, Labhasetwar V. TAT-conjugated nanoparticles for the CNS delivery of anti-HIV drugs. Biomaterials. 2008;29(33):4429–38.
20. Torchilin VP. Tat peptide-mediated intracellular delivery of pharmaceutical nanocarriers. Adv Drug Deliv Rev. 2008;60(4):548–58.
21. Kamei N, Morishita M, Takayama K. Importance of intermolecular interaction on the improvement of intestinal therapeutic peptide/protein absorption using cell-penetrating peptides. J Contr Release. 2009;136(3):179–86.
22. Zhao P, Wang H, Yu M, Cao S, Zhang F, Chang J, *et al.* Paclitaxel-loaded, folic-acid-targeted and TAT-peptide-conjugated polymeric liposomes: in vitro and in vivo evaluation. Pharm Res. 2010;27(9):1914–26.
23. Jiang QY, Lai LH, Shen J, Wang QQ, Xu FJ, Tang GP. Gene delivery to tumor cells by cationic polymeric nanovectors coupled to folic acid and the cell-penetrating peptide octaarginine. Biomaterials. 2011;32:7253–62.
24. Pujals S, Fernández-Carneado J, López-Iglesias C, Kogan MJ, Giralt E. Mechanistic aspects of CPP-mediated intracellular drug delivery: relevance of CPP self-assembly. Biochimica et Biophysica Acta (BBA)-Biomembr. 2006;1758(3):264–79.
25. Harush-Frenkel O, Bivas-Benita M, Nassar T, Springer C, Sherman Y, Avital A, *et al.* A safety and tolerability study of differently-charged nanoparticles for local pulmonary drug delivery. Toxic Appl Pharm. 2010;246(1):83–90.
26. Hoet PH, Brüske-Hohlfeld I, Salata OV. Nanoparticles-known and unknown health risks. J Nanobiotechnology. 2004;2(1):12.
27. Gao H, Xiong J, Cheng T, Liu J, Chu L, Liu J, *et al.* In Vivo Biodistribution of Mixed Shell Micelles with Tunable Hydrophilic/Hydrophobic Surface. Biomacromolecules. 2013;14(2):460–7.
28. Takakura Y, Fujita T, Hashida M, Sezaki H. Disposition characteristics of macromolecules in tumor-bearing mice. Pharm Res. 1990;7(4):339–46.
29. Wang Y, Wang Y, Xiang J, Yao K. Target-specific cellular uptake of taxol-loaded heparin-PEG-folate nanoparticles. Biomacromolecules. 2010;11(12):3531–8.
30. Tran TH, Bae BC, Lee YK, Na K, Huh KM. Heparin-folate-retinoic acid bioconjugates for targeted delivery of hydrophobic photosensitizers. Carbohydr Polymer. 2012;92:1615–24.
31. Scomparin A, Salmaso S, Bersani S, Satchi-Fainaro R, Caliceti P. Novel folated and non-folated pullulan bioconjugates for anticancer drug delivery. Eur J Pharm Sci. 2011;42(5):547–58.
32. Yoo HS, Park TG. Folate-receptor-targeted delivery of doxorubicin nano-aggregates stabilized by doxorubicin-PEG-folate conjugate. J Contr Release. 2004;100(2):247–56.
33. Sawant R, Torchilin V. Intracellular delivery of nanoparticles with CPPs. Methods Mol Biol. 2011;683:431–51.
34. Wang X, Li J, Wang Y, Cho KJ, Kim G, Gjyrezi A, *et al.* HFT-T, a targeting nanoparticle, enhances specific delivery of paclitaxel to folate receptor-positive tumors. ACS Nano. 2009;3(10):3165–74.
35. Sahay G, Alakhova DY, Kabanov AV. Endocytosis of nanomedicines. J Control Release. 2010;145(3):182–95.
36. Zhang LW, Monteiro-Riviere NA. Mechanisms of quantum dot nanoparticle cellular uptake. Toxicol Sci. 2009;110(1):138–55.
37. Iversen T-G, Skotland T, Sandvig K. Endocytosis and intracellular transport of nanoparticles: Present knowledge and need for future studies. Nano Today. 2011;6(2):176–85.
38. Wang F, Wang Y-C, Dou S, Xiong M-H, Sun T-M, Wang J. Doxorubicin-tethered responsive gold nanoparticles facilitate intracellular drug delivery for overcoming multidrug resistance in cancer cells. Acs Nano. 2011;5(5):3679–92.
39. Schiff PB, Horwitz SB. Taxol stabilizes microtubules in mouse fibroblast cells. Proc Natl Acad Sci. 1980;77(3):1561–5.